ADVANCED OPTICAL MATERIALS

www.advopticalmat.de

Active Control of Resonant Cloaking in a Terahertz MEMS Metamaterial

*Manukumara Manjappa, Prakash Pitchappa, Nan Wang, Chengkuo Lee, and Ranjan Singh**

Metamaterials exhibiting exotic optical properties have played a significant role over the years in guiding the concept of invisibility cloaking from the realm of being fiction to reality. However, due to the difficulties in fabricating the 3D cloaking devices and lack of exotic plasmonic materials at terahertz (THz) frequencies, the experimental realization of cloaking phenomenon in the THz spectrum is challenging. In this work, a new mechanism for invisibility cloaking based on the resonant scattering cancellation technique in a 2D nonconcentric composite metamaterial device, consisting of a split ring resonator (SRR) and a microelectromechanical system (MEMS) reconfigurable closed ring resonator (CRR) at THz frequencies is reported. A strong magnetic interaction between the SRR and CRR eliminates the scattering effects from the SRR at its fundamental eigen mode frequency, thereby making it invisible to the incident THz wave. Further, by voltage actuation of MEMS-reconfigurable CRR, an active switching between the visible and cloaked states of SRR structure is demonstrated. The proposed technique provides a simple design and technique for realizing invisibility cloaks by utilizing the resonant near-field interactions in the subwavelength structures across microwave to optical frequencies, thereby circumventing the need for materials with complex geometry and exotic properties.

Competence of engineering the effective material properties like permittivity and permeability of a medium using the electromagnetic metamaterials has inspired many fascinating aspects in science. These include the pioneering concept of super lens,[1,2] negative refraction,[3] invisibility cloaking,[4–8] artificial magnetism,[9] and many more. Particularly, the experimental demonstration of invisibility cloak in the microwave[10,11] and optical frequencies,[12–15] which was once just a science fiction, has been the hallmark achievement of metamaterials and optics in recent times. In general, the concept of invisibility implies reduction or cancellation of the scattering effects of the material of interest (also referred to as principal scatterer), which can be realized by tailoring the effective parameters such as permittivity and permeability of the surrounding medium. Over the years several cloaking techniques have been proposed using metamaterials and plasmonic structures[16] that mainly include scattering cancellation technique (SCT),[17–21] transmission line technique,[22] transformation optics,[4–8,23,24] quasi-conformal mapping techniques,[24,25] and anomalous localized resonances in plasmonic structures.[26] In particular, SCT provides a simple design and structure without the need for complex geometries to realize invisibility effects across the infrared and visible frequencies. In SCTs, the low-loss isotropic plasmonic/metamaterial cover (also referred to as induced scatterer) operating at near plasmon frequencies is used to drastically reduce the scattering cross-section of the principal scatterer. The condition for SCT dictates that the metamaterial cover and the principal scatterer should possess contrasting dielectric constants to induce opposing polarizabilities.[18] Hence, for a proper choice of the radius of metamaterial cover, the induced opposing dipoles on the metamaterial cover cancel out the dipoles of the principal scatterer, thereby making it invisible to the incident light. Despite the favorable features such as nonresonant and isotropic nature of the SCT-based invisibility effects, the requirement on the choice of materials possessing relatively low permittivity ($\varepsilon_r < 1$) values makes it extremely difficult to realize across the broad range of electromagnetic frequencies.

Terahertz (THz) part of the electromagnetic spectrum is regarded as the technologically significant spectral domain

M. Manjappa, Dr. P. Pitchappa, Prof. R. Singh
Division of Physics and Applied Physics
School of Physical and Mathematical Sciences
Nanyang Technological University
21 Nanyang Link, Singapore 637371, Singapore
E-mail: ranjans@ntu.edu.sg

M. Manjappa, Dr. P. Pitchappa, Prof. R. Singh
Centre for Disruptive Photonic Technologies
The Photonics Institute
Nanyang Technological University
50 Nanyang Avenue, Singapore 639798, Singapore

Dr. N. Wang
Institute of Microelectronics
11 Science Park Road, Singapore 117685, Singapore

Prof. C. Lee
Department of Electrical & Computer Engineering
National University of Singapore
4 Engineering Drive 3, Singapore 117576, Singapore

Prof. C. Lee
Center for Intelligent Sensors and MEMS (CISM)
National University of Singapore
E6 #05-11F, 5 Engineering Drive 1, Singapore 117608, Singapore

The ORCID identification number(s) for the author(s) of this article can be found under https://doi.org/10.1002/adom.201800141.

DOI: 10.1002/adom.201800141

that bridges the gap between the high speed electronics and photonics. Most of the cloaking techniques proposed so far rely on either the choice of cloaking material possessing exotic properties or complex 3D design requirements, which makes it extremely difficult to realize the invisibility cloak effects in the THz part of the electromagnetic spectrum. One of the first experimental demonstrations on invisibility cloak at THz frequencies was shown using a triangular 3D cloak fabricated by using the projection microstereolithography process.[27] Recently, few designs based on the 3D carpet cloak in the THz frequencies were proposed, however they are difficult and nontrivial to realize experimentally.[28] One of the possible ways to circumvent the existing limitations is to extract the strong resonant interactions within the composite medium in planar 2D structures to drastically eliminate the scattering effect of one of the resonant structures, which works on the principle of SCT to make the resonant structure invisible to the incoming beam. Realizing 2D designs for the cloaking devices enable easy and large area fabrication that would enhance the possibility of practical realization of cloaking effects of the large samples across broad frequency spectrum. In this regard, 2D metamaterials that offer strong near-field interactions can provide a good platform to realize resonant invisibility cloaking devices across broad range of frequency spectrum ranging from microwave to optical frequencies.

Here, we propose and experimentally demonstrate resonant scattering cancellation technique to realize invisibility cloaking of a resonant structure under the influence of the strong near-field interaction in a 2D composite reconfigurable metamaterial medium. The induced magnetic coupling between the split ring resonator (SRR) and the closed ring resonator (CRR) creates a strong magnetic dipole that cancels out the opposing resonant magnetic dipole of the SRR, thereby making the SRR invisible to the incoming THz wave. Unlike the traditional SCT device that depends on the dielectric properties of the materials, the proposed composite metamaterial design uses the bianisotropy nature of the resonant SRR and the induced magnetic dipoles in realizing the invisibility effect within the device. Further, by adding an active structural reconfiguration feature to the CRR design through an electrically tunable microelectromechanical system (MEMS), we show a voltage-controlled active switching between the visible and cloaked states of the SRR structure to the incident THz wave. MEMS cantilever-based metamaterial provides unique prospects including active control of structural and optical properties of the metamaterial system, thereby enhancing their technological relevance. Previous demonstrations using MEMS designs have shown active control of chirality,[29] anisotropy,[30] perfect absorption,[31] logical operations,[32] and phase engineering[33] in the system using either the thermal[34,35] or electrical/voltage controls.[36] In this work, we show active control of the MEMS-actuated CRR structure using voltage in the out-of-plane direction of the sample that enables precise and dynamic control of the effective parameters of the metamaterial medium, thereby actively switching the cloaking effect in the system. In the literature, there are several works demonstrating the active control of metamaterial resonances using semiconductors such as GaAs,[37] silicon,[38] perovskites,[39] and other dynamic materials. However, MEMS offer distinctive feature of out-of-plane reconfiguration of metamaterial structure that allows us to probe and dynamically manipulate the near fields extended in the third dimension (z-axis) of the sample. By actuating the MEMS CRR structure in the third dimension through voltage control, we actively tune the bianisotropy in the proposed system to switch between the visible and cloaked states of the SRR, unlike the other planar devices including the previously studied concentric and nonconcentric composite metamaterial structures.[40–42]

The proposed 2D reconfigurable metamaterial structure is composed of a SRR placed nonconcentrically within a MEMS-actuated CRR. An artistic representation of the MEMS-actuated cloaking device is presented in **Figure 1**, where in the snapped down (ON) state of the outer CRR structure, the resonant SRR structure becomes invisible to the incident THz waves. The scanning electron microscope (SEM) image of the fabricated sample is shown in the left inset of the Figure 1. The device is fabricated using the complementary metal–oxide–semiconductor (CMOS) compatible process. The metamaterial is made of varying thicknesses of aluminium (Al) (t = 300, 500, 700, and 900 nm) on top of 50 nm aluminum oxide (Al_2O_3) deposited on the silicon substrate. The selective part of CRR is released by isotropically etching away the sacrificial silicon-dioxide (SiO_2) layer from underneath the bimorph structure. Due to the residual stress in the bimorph layers, the cantilevers are bent up (released state), thereby creating an enhanced air gap

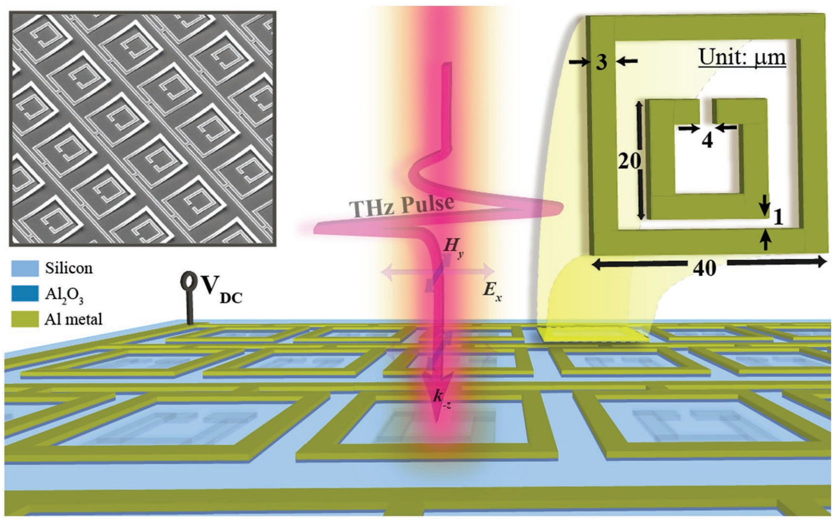

Figure 1. Artistic representation of the MEMS-incorporated composite reconfigurable metamaterial structure consisting of outer MEMS closed ring resonator (CRR) and the inner split ring resonator (SRR), where the latter becomes invisible to the incoming THz wave in the ON (V_{DC} = 30 V) state of the device. Left inset shows the scanning electron microscope (SEM) image of the fabricated composite MEMS metamaterial device in its released (OFF, V_{DC} = 0 V) state. The right inset depicts the unit cell dimensions of the metamaterial design with a square period of 50 µm. The metallic interconnects to the CRR are not shown in the SEM inset for clarity of the image.

between the substrate and bimorph cantilevers, as shown by the SEM image of the sample in the inset of Figure 1 (details on the design and fabrication process are given in the Experimental Section). The unit cell dimensions of the sample are given in the right inset of Figure 1, where the total length of SRR is half that of the MEMS-actuated CRR, with their metal arms separated by a coupling distance of d = 1 µm, when the device is in ON state. The out-of-plane actuation of the released arm of the CRR structure is achieved through electrostatic control, by applying voltage (V_{DC}) across the Al metal lines and low resistivity silicon substrate (>1 Ω cm). The Al_2O_3 layer in the bimorph (Al_2O_3/Al) structure electrically isolates the metal interconnect lines and the Al layer of CRR cantilevers from the substrate when the device is in its ON state and this allows for the voltage controlled out-of-plane actuation of the CRR cantilevers.

The fabricated composite MEMS metamaterial device is experimentally characterized using the terahertz time domain spectroscopy (THz-TDS) system for both ON (snapped) and OFF (released) configurations of the device at the normal incidence angle of the THz wave that is polarized parallel ($\boldsymbol{E}_x$) to the gap bearing arm of the SRR (measurement procedures are provided in the Experimental Section). The measured THz transmission spectra for the ON and OFF voltage states of the device are given in **Figure 2**a along with the corresponding SEM image of the device configuration. As shown, in the OFF (released, V_{DC} = 0 V) state of the CRR cantilevers, the transmission spectrum exhibits a strong coupling behavior signifying the mode hybridization of the SRR and the CRR resonances leading to a narrow band transmission peak at 1.1 THz. This configuration represents the widely studied metamaterial-induced transparency effect,[40–42] where the sharp inductive–capacitive (LC) resonance feature of the SRR and the broad dipole resonance of the CRR appearing at the same resonance frequency exhibit Fano-type of destructive interference mechanism, leading to a sharp transmission window at the resonance frequency.[43] The appearance of transparency peak in the spectrum signifies a strong influence of the eigen (LC) resonance of the SRR in the composite MEMS metamaterial structure. As the CRR cantilever is snapped down (ON state, V_{DC} = 30 V) on the substrate, the transparency peak completely disappears and a strong dipole type of resonance is observed in the transmission spectrum (shown by the red line). Numerical simulations were carried out using the computer simulation technology (CST) microwave studio frequency solver to precisely elucidate the near- and far-field optical characteristics of the metamaterial structure for the ON (snapped) and OFF (released) states of the CRR cantilevers and the corresponding transmission spectra are shown in Figure 2b. The material parameters and the numerical methods followed in the simulations are

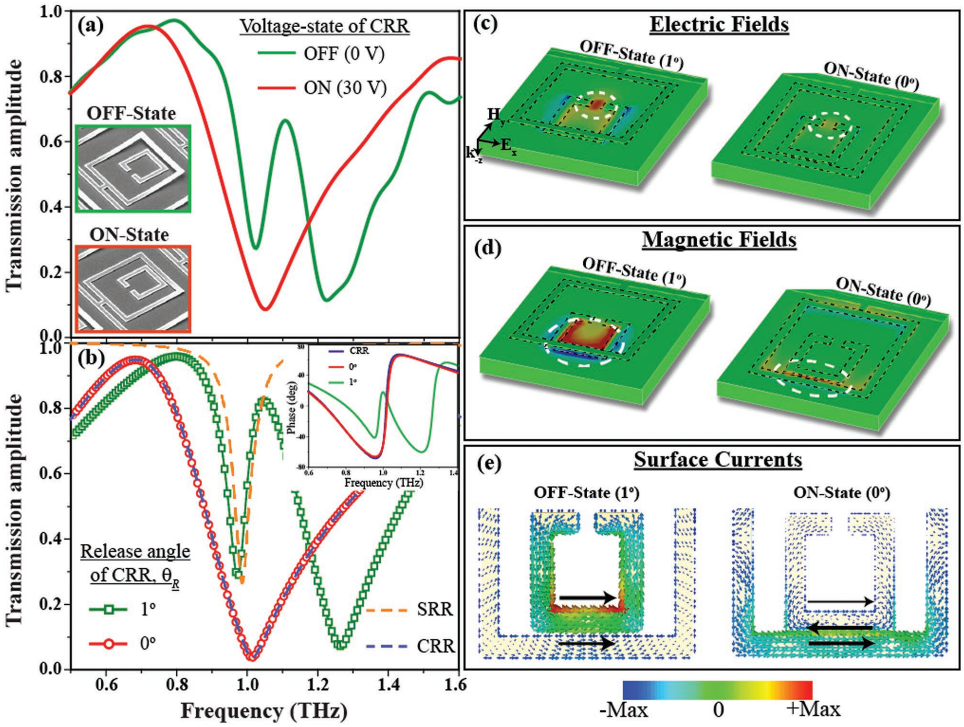

Figure 2. a) Experimentally measured THz transmission spectra of the composite MEMS-metamaterial device without (green line) and with (red line) the voltage (V_{DC}) applied across the metal lines and the silicon substrate. The measurements were performed on the sample with the metal thickness t = 900 nm. The insets show SEM images of OFF and ON states of the metamaterial with V_{DC} = 0 and 30 V, respectively. b) Depicts the numerically simulated THz transmission spectra for the composite MEMS metamaterial and the individual CRR and SRR. The spectrum for the release angle of CRR (θ_R) of 1° and 0° respectively correspond to the OFF and ON states of the experimentally measured data shown in inset (a). The inset represents the phase spectra of the transmitted THz wave for CRR alone and ON/OFF state of the composite MEMS metamaterial device. c) Electric field, d) magnetic field, and e) surface current distributions shown for the OFF and ON state of the MEMS metamaterial highlighting the cancellation of SRR fields in the ON state.

described in the Experimental Section. The voltage states (V_{DC}) in the experiments can be expressed in terms of release angle (θ_R) of the CRR cantilever, where V_{DC} = 0 V (OFF) and 30 V (ON) corresponds to θ_R = 1° (released, OFF) and 0° (snapped, ON), respectively. The curves shown in green squares and the red circles represent the OFF (1°) and the ON (0°) states of the CRR cantilever in the composite structure and are in good agreement with the corresponding measured spectra shown in Figure 2a. Further, simulations were carried out for the individual (uncoupled) SRR and the CRR structures possessing the same unit cell dimensions and periodicity as specified in Figure 1 and the resulting transmission spectra are shown by orange-dash and blue-dashed lines, respectively in Figure 2b. Particularly, the LC resonance feature of SRR coincide with the low frequency hybridized mode of the composite MEMS metamaterial in the OFF state (θ_R = 1°) of CRR, whereas in the ON state (θ_R = 0°), the dipole resonance of CRR alone precisely overlaps with the observed broad dipole type feature in the composite MEMS metamaterial. Further, the phase of the propagating wave passing through the composite MEMS metamaterial for ON (θ_R = 0°) state shows no distortion with respect to the phase of the wave passing through the CRR alone, as shown in the inset of Figure 2b. On the other hand, for OFF state (θ_R = 1°) of composite MEMS metamaterial due to the influence of SRR scattering, the phase profile and hence the wavefront of the propagating THz wave is strongly altered (shown by green line). This confirms that the SRR present in the composite MEMS metamaterial in the ON state of the device does not alter the phase or wavefront of the propagating THz waves, and thus becomes invisible. This far-field observation clearly highlights annihilation of the SRR effect under the influence of strong near-field magnetic coupling with the adjacent CRR arm.

Cancellation of the SRR effect seen at the far-field spectra is further supported and clearly elucidated by the nature of near-field electric, magnetic, and surface current distributions shown in Figure 2c–e for OFF and ON states of the composite MEMS metamaterial. In the OFF (released) state, the electric and magnetic fields are confined in the gap and around the metal arm of the SRR structure, respectively, indicating a strong resonant interaction of the SRR with the incoming THz wave of polarization $\boldsymbol{E}_x$. As the CRR is snapped down onto the substrate, with the separation (d) between the SRR inductive arm and CRR arm being 1 µm, the confined electric and magnetic fields within the SRR structure disappears, thereby making the resonant SRR structure invisible to the incident $\boldsymbol{E}_x$ polarized THz wave. The mechanism of the observed resonant invisibility is understood by studying the surface current distributions shown in the Figure 2e. In the OFF state, SRR shows a strong surface current distribution, signifying a stronger coupling of SRR with the incident THz wave, where most of the near-field energy is confined within the SRR structure. In the ON state, once the inductive arm of the SRR is in a close proximity (d = 1 µm) of the CRR arm, strong opposing currents develop on the outer edge of the SRR and the CRR arms. These currents give rise to a strong magnetic interaction thereby inducing a magnetic field between the SRR and CRR arms with their magnetic dipoles aligned perpendicular ($\boldsymbol{H}_z$) to the plane of the sample. The induced surface current (magnetic dipole) possesses the opposite sign and greater strength with respect to the intrinsic surface currents (magnetic field) of the SRR structure, thereby cancelling the surface currents (near-field effects) of the SRR structure. Further insights on magnetic interactions in the composite metamaterial structure have been discussed in our previous study[42] that relates the cancellation of the SRR effect to the ratio of the magnetic fields and the phase reversal point of the magnetic dipoles in the strong magnetic coupling regime of the medium. Hence, a strong resonant magnetic interaction between the SRR (principal scatterer) and the CRR (induced scatterer) results in the cancellation of SRR magnetic dipole, thereby making it invisible to the incoming THz wave, which is a resonant magnetic analogue to the scattering cancellation techniques widely proposed for realizing the cloaking effects using the plasmonic structures.

Further studies were carried out to understand the influence of the coupling effects in the composite MEMS metamaterial on the transmission characteristics and the effective parameters of the medium for varying metal thicknesses (t) and the corresponding release angle (θ_R) of the CRR structure. In **Figure 3**a,

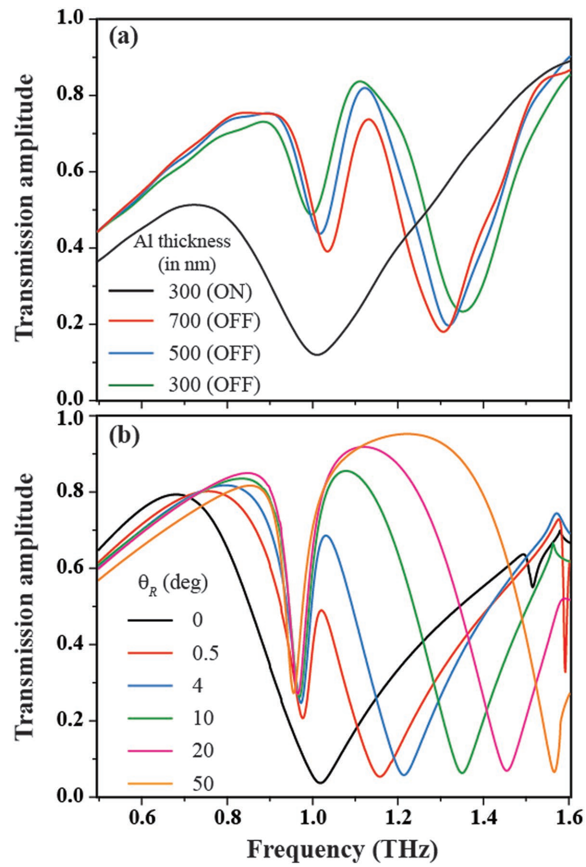

Figure 3. a) Depicting the experimentally measured THz transmission spectra for the composite MEMS metamaterials possessing different metal thicknesses (t = 300, 500, and 700 nm) in their OFF state and for 300 nm thick metal in its ON state. b) Numerically simulated transmission spectra for the composite MEMS metamaterial for varying release angle (θ_R) of the outer CRR structure. The change in the metal thickness of the CRR inversely corresponds to the change in the release angles—thinner the metal, higher is the release angle of CRR.

the measured transmission spectra for varying metal thicknesses (t) are shown, where with decreasing t in the released state of the sample, the spectra exhibit mode hybridization characteristic possessing gradual increase in LC resonance strength and blue shift in the frequency of the dipole resonance of the CRR structure. Change in the metal thickness corresponds to the change in the release angle of the CRR, where thinner metal will result in larger release angle of the cantilever of the same length.[44] Hence, in the OFF state, the device with 300 nm metal thickness will possess larger release angle (θ_R) and hence larger blue shift in the dipolar resonance of CRR structure. To further support this observation, numerical simulations were carried out by varying the release angle (θ_R) of the CRR cantilever and the resulting transmission spectra are shown in Figure 3b. For $\theta_R = 0$, the transmission spectrum shows a broad dipolar resonance and with increasing θ_R, it exhibits similar behavior as observed in the experiments that shows gradual increase in the strength of the LC resonance of SRR and large blue shift in the dipole resonance of the CRR for the angle of $\theta_R = 50°$. At this larger release angle the SRR decouples from the strong magnetic influence of the CRR arm and hence becomes visible as it interacts strongly with the incoming THz wave.

It is well established that the major factors governing the invisibility cloaking effects are the effective parameters of the medium such as electric permittivity (ε) and magnetic permeability (μ). Here to further support our claims, we extract the complex permittivity ($\varepsilon = \varepsilon_{Re} + i\ \varepsilon_{Im}$) and permeability ($\mu = \mu_{Re} + i\ \mu_{Im}$) of the composite MEMS metamaterial for varying θ_R of CRR as discussed in Figure 3b. The effective parameters of the medium were calculated using the expression for the impedance (z) and the refractive index (n) discussed in Ref. [45], by using the scattering (S) parameters S_{11} (reflected) and S_{21} (transmitted) extracted from the numerical simulations. Later, the complex electric permittivity and complex magnetic permeability were calculated by using the formula $\varepsilon = \frac{n}{z}$ and $\mu = n \cdot z$, respectively and are plotted in **Figure 4** for varying θ_R of CRR. For $\theta_R = 0°$, a broad resonance spectrum near 1 THz is seen that exhibits strong magnetic response resulting in anomalous change in the magnetic permeability of the medium (black line in Figure 4c,d), on the other hand, the electric permittivity of the medium shows no response (black line in Figure 4a,b) at the resonance. This result justifies that the broad resonance feature in the composite MEMS metamaterial is rich in the magnetic response due to the strong magnetic interactions between the inductive arm of the SRR and the CRR arm in the ON state ($\theta_R = 0°$) of the device, that results from the strong bianisotropy in the system. Hence, in this configuration (i.e., $\theta_R = 0°$), the composite device behaves as a magnetic medium showing the negative values for Re(μ) in some part of the frequencies near the resonance as shown in Figure 4c. As the release angle (θ_R) is increased, the magnetic permeability (μ) of the medium gradually decreases, meanwhile the response of electric permittivity (ε) in the medium starts to grow stronger in strength. At larger angle (i.e., $\theta_R = 50°$), the electric permittivity in the medium dominates the resonance response (orange line in Figure 4a,b), whereas the strength of magnetic permeability (μ) becomes insignificant and the Re(μ) takes the positive values (orange line in Figure 4c) signifying annihilation of magnetic response in the system. This observation is true since, at the larger angles, the SRR resonance starts to show the dominating effects, where these effects are dominated by the electric response and hence shows negative values and anomalous change in the Re(ε). Therefore, by actively tuning the release angle (θ_R) of the CRR cantilevers using the voltage input, enables the gradual switching between the electric and magnetic response of the composite MEMS metamaterial thereby aiding the dynamic control of the invisibility cloaking effect in the system.

The effect of incidence angle on the cloaked state of the device is illustrated in **Figure 5**, where we present the numerically calculated far-field transmission response and the near-field energy distribution in the composite MEMS metamaterial for varying angle of incidence (θ_x, θ_y) of the incoming THz beam. Angle of incidence of the THz beam is separately varied along the x- (θ_x) and the y-axis (θ_y) of the sample. For θ_x variation, the H-component of the THz wave always remain in the plane (along y-axis) of the sample and the E-component forms a projection along the z-axis (out-of-plane) of the

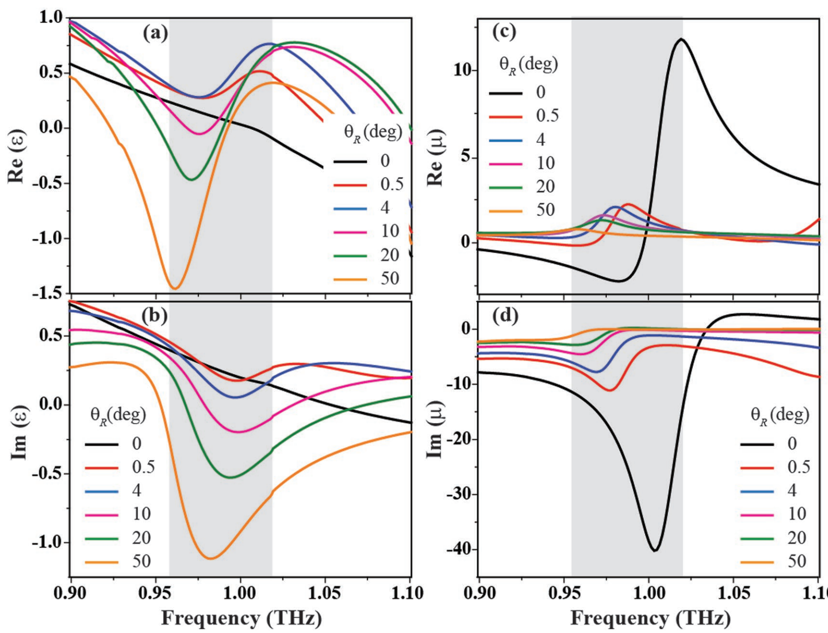

Figure 4. Numerically extracted a,c) real and b,d) imaginary parts of effective permittivity (ε) and permeability (μ) of the composite MEMS metamaterial medium for varying release angles (θ_R) of CRR, respectively. The medium exhibits strong magnetic response in its ON (cloaked) state (black line in (c) and (d)), where the electric response is negligible (black line in (a) and (b)). In the OFF (released) state, as the release angle (θ_R) increases, the electric response of the medium dominates (orange line in (a) and (b)) and the magnetic response diminishes (orange line in (c) and (d)) at the resonance.

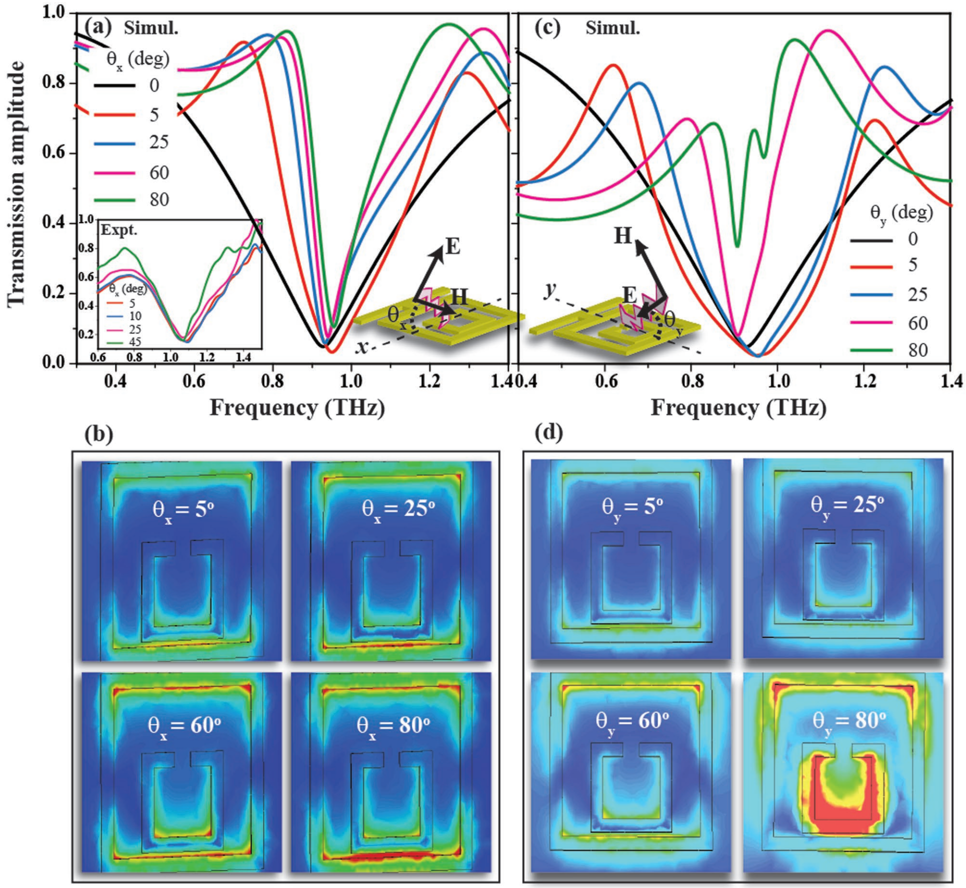

Figure 5. Numerically simulated a) THz transmission spectra and b) magnetic field distributions for the composite MEMS metamaterial sample for varying angle of incidence (θ_x) of the THz beam along the x-axis, which respectively shows narrowing of the resonance and increase in the strength of magnetic interactions between SRR and CRR for increasing θ_x. The inset figure in (a) depicts the measured transmission spectrum through the composite MEMS metamaterial sample for varying θ_x. c,d) The numerically calculated transmission spectra and the magnetic field distribution for the varying angle of incidence (θ_y) along y-axis showing the reappearance of SRR effect for large angle ($\theta_y = 80°$).

sample, whereas for θ_y variation, the E-component of the THz wave remains in the plane (along x-axis) and the H-component forms a projection along the z-axis (out-of-plane) of the sample. Varying the incidence angle (θ_x) by keeping the H-component of THz wave in the plane of the sample results in the gradual decrease of resonance linewidth in the far-field transmission spectra with no significant change in its resonance amplitude, as shown in Figure 5a. Meanwhile, the near-field confinement of the magnetic distribution for varying θ_x shown in Figure 5b highlights gradual increase in the magnetic field confined in the region between the SRR and CRR arms, which therefore results in the significant reduction of the linewidth of the far-field resonance spectra (Figure 5a). Absence of the magnetic field confinement within the SRR for increased incident angles θ_x affirms that the invisibility of SRR is insensitive (independent) to angle of incidence (θ_x) along the x-axis of the sample. The experimentally measured far-field transmission spectra for varying angle of θ_x are shown in the inset of Figure 5a that match well with the resonance narrowing trend seen in the simulation data, where for $\theta_x = 45°$ (green line), the linewidth of the resonance becomes narrower than for the angle $\theta_x = 5°$ (red line). On the other hand, when the angle of incidence is varied along the y-axis (θ_y), linewidth of the far-field spectra becomes narrower till $\theta_y < 80°$, as shown in Figure 5c, which shows a similar trend in the resonance behavior seen for θ_x variation. At $\theta_y = 80°$, the far-field spectrum shows a strong mode splitting characteristic (green line, Figure 5c) indicating reappearance of SRR response in the composite MEMS metamaterial that can be clearly shown by the enhanced magnetic fields near the inductive arm of the SRR shown in Figure 5d for $\theta_y = 80°$. At large θ_y, rather than the electric (E)-component of the THz wave, it is the magnetic (H)-component of the field that directly excites the SRR in the system, thereby making it visible to the incident THz wave. The optical response of the sample at larger incident angle (θ_x and $\theta_y > 45°$) is not realistic in the experimental conditions at THz frequencies, because of the violation of effective and homogenous medium conditions for the fabricated planar sample. Hence, the reported resonant invisibility of SRR structure to the THz wave with an added advantage of insensitiveness to the angle of incidence benefits the realization of plasmonic/metamaterial coupling induced cloaking devices at terahertz and higher frequencies, which operates on the principle of resonant scattering cancellation techniques.

In summary, we demonstrated an active resonant invisibility of SRR in a 2D planar MEMS metamaterial device composed of nonconcentric SRR and CRR structures at terahertz frequencies. We showed that a strong magnetic interaction between the SRR (principal scatterer) and the CRR (induced scatterer) induces the cancellation of magnetic dipole of the SRR. Active switching between the visible and cloaked states of the SRR structure using the voltage states $V_{DC} = 0$ and 30 V, respectively, was experimentally demonstrated. Further, active tailoring of the medium parameters such as permittivity and permeability, showed that the device can be switched from magnetic medium to nonmagnetic medium with permeability values of the medium changing from negative to positive values. The reported invisibility effects depend on the polarization of the incoming THz beam due to the structural anisotropic nature of the SRR (principal scatterer) itself; however, they are insensitive to the incidence angle of the incoming beam. Moreover, the proposed technique provides a new platform to realize active control of invisibility cloaking phenomena in planar metamaterials across the wide range of electromagnetic spectrum. The results show useful prospects in real world applications as resonant switches, active slow-light devices, modulators and active band pass filters across terahertz frequencies.

Experimental Section

Design: The chosen design of placing the SRR and CRR in the nonconcentric arrangement (coupling distance $d = 1$ µm) enabled strong inductive (magnetic) interactions in the system that was greater than the strength of the magnetic dipole in the SRR structure. This created stronger and opposing scattering fields in the vicinity of the SRR (principal) scatterer that canceled the weakly scattered fields from the SRR, thereby making it invisible to the resonant THz wave. These were subwavelength structures and the spectroscopically probed area of metamaterial medium consisting of nearly 5028 resonators arranged periodically within the spot size (4 mm) of the incident THz beam, which satisfied the homogeneity condition to enhance the strength of cloaking effects seen in the far-field for a single composite metamolecule unit cell of periodicity 50 µm.

Fabrication Process: The composite MEMS metamaterial was fabricated using a CMOS compatible process as described below. First, the lightly doped 8" low resistivity silicon substrate of 725 µm thickness was cleaned and a 100 nm thick sacrificial SiO_2 layer was deposited using low pressure chemical vapor deposition (LPCVD) process. Following this, conventional photolithography process was used to pattern the anchor region. With the designed pattern, the parts of sacrificial SiO_2 for anchor regions were dry etched using reactive ion etching process. After this, a 50 nm thick Al_2O_3 layer was deposited using the atomic layer deposition (ALD) process, followed by the sputter deposition of 300, 500, 700, and 900 nm thick Al. Note that the bimorph layers (Al/Al_2O_3) were in physical contact with Si substrate at the anchor region, and in the remaining part of the wafer, it was on top of sacrificial SiO_2 layer. Then, the second photolithography step was carried out for defining the cantilevers and metal lines of metamaterial patterns. Following this, both Al and Al_2O_3 layers were dry etched to form the designed metamaterial. Finally, vapor hydrofluoric acid (VHF) was used to isotropically etch the SiO_2 sacrificial layer underneath the bimorph structures, thereby suspending it over the Si substrate with an air gap between them. At the anchor region, since the bimorph cantilevers were in physical contact with Si substrate, the VHF release process was not time controlled, and this ensured higher yield of the devices. Due to the residual stress in the bimorph cantilevers of CRR structure, the released cantilevers were bent up, thereby increasing the initial tip displacement.

THz Measurements: The composite MEMS metamaterials were optically characterized using the conventional GaAs photoconductive switch based THz-time domain spectroscopy system operating in the transmission mode. The wire-bonded metamaterial sample was positioned at the focus of the THz beam. The electrical connections to the CRR structures were established using a DC voltage source. The measurements were performed for the voltage states of $V = 0$ V (OFF) and $V = 30$ V (ON) applied on the CRR cantilever with the THz wave of beam spot 4 mm incident at the normal angle on the sample and the transmitted THz pulse was captured using the THz detector connected to the lock-in amplifier. THz response through the bare silicon substrate was measured for referencing the signal through the sample. In the post processing steps, the detected THz pulses measured through the sample and the bare substrate were fast Fourier transformed (FFT) to obtain the corresponding THz spectra. Later, the transmitted THz spectrum through the sample ($T_s(\omega)$) was normalized with respect to the transmission through the substrate ($T_R(\omega)$), i.e., $T(\omega) = T_s(\omega)/T_R(\omega)$ and the normalized spectrum is shown in the Figures 2a and 3a.

Numerical Simulations: Finite-difference time-domain (FDTD) numerical simulations were conducted to calculate the far-field THz transmission spectra and the confined electric near-fields and surface current distributions showing the visible and invisible (cloaked) states of the SRR for the $\boldsymbol{E}_x$ polarization of the THz wave. Full-field electromagnetic wave simulations were performed using the commercial simulation software CST microwave studio. For the material property, aluminum (Al) of varying thickness 300, 500, 700, and 900 nm were modeled as lossy metal with conductivity of 3.57e7 S m^{-1}. Aluminum oxide and silicon were modeled as lossless dielectric materials with dielectric constant of 9.5 and 11.9, respectively. In the simulation, a single unit cell of the metamaterial structures was simulated with unit cell boundary conditions employed in axial directions orthogonal to the incident waves. The perfectly matched layers were applied along the propagation of the electromagnetic waves. Plane waves were incident into the unit cell from the port on the metal side, while the transmission spectrum was determined from the probe placed at the other side of metamaterial. The deformation angles for the cantilevers were used to tilt the metal cantilevers that established the congruence between the values of applied voltages (V) and the release angle (θ_R) used in the simulations. In the meanwhile, field monitors were used to collect the electric fields, magnetic fields, and the respective surface currents at 1 THz frequency for $\theta_R = 1°$ (released, OFF) and 0° (snapped, ON) states of the device.

Acknowledgements

Authors thank Willie Padilla, Shuvan Prahanth and Yihao Yang for their fruitful discussions and the reviewers for their inputs on the work. M.M., P.P., and R.S. acknowledge the funding support from Ministry of Education, Singapore MOE2016-T3-1-006 and MOE2017-T2-1-110 grants and the National Research Foundation (NRF), Singapore and Agence Nationale de la Recherche (ANR), France NRF2016-NRF-ANR004 (M4197003) grant. C.L. acknowledges the grant support from NRFCRP15-2015-02 "Piezoelectric Photonics Using CMOS Compatible AlN Technology for Enabling The Next Generation Photonics ICs and Nanosensors" at NUS, Singapore.

Conflict of Interest

The authors declare no conflict of interest.

Keywords

invisibility cloaking, MEMS metamaterial, resonant switching, terahertz

Received: February 2, 2018
Revised: May 3, 2018
Published online:

[1] J. B. Pendry, *Phys. Rev. Lett.* **2000**, *85*, 3966.
[2] N. Fang, H. Lee, C. Sun, X. Zhang, *Science* **2005**, *308*, 534.
[3] D. R. Smith, J. B. Pendry, M. C. K. Wiltshire, *Science* **2005**, *305*, 788.
[4] U. Leonhardt, *Science* **2006**, *312*, 1777.
[5] J. B. Pendry, D. Schurig, D. R. Smith, *Science* **2006**, *312*, 1780.
[6] U. Leonhardt, T. Tyc, *Science* **2009**, *323*, 110.
[7] J. Li, J. B. Pendry, *Phys. Rev. Lett.* **2008**, *101*, 203901.
[8] H. Chen, C. T. Chan, P. Sheng, *Nat. Mater.* **2010**, *9*, 387.
[9] T. J. Yen, W. J. Padilla, N. Fang, D. C. Vier, D. R. Smith, J. B. Pendry, D. N. Basov, X. Zhang, *Science* **2004**, *303*, 1494.
[10] D. Schurig, J. J. Mock, B. J. Justice, S. A. Cummer, J. B. Pendry, A. F. Starr, D. R. Smith, *Science* **2006**, *314*, 977.
[11] N. Landy, D. R. Smith, *Nat. Mater.* **2013**, *12*, 25.
[12] W. Cai, U. K. Chettiar, A. V. Kildishev, V. M. Shalaev, *Nat. Photonics* **2007**, *1*, 224.
[13] T. Ergin, N. Stenger, P. Brenner, J. B. Pendry, M. Wegener, *Science* **2010**, *328*, 337.
[14] J. Valentine, J. Li, T. Zentgraf, G. Bartal, X. Zhang, *Nat. Mater.* **2009**, *8*, 568.
[15] L. H. Gabrielli, J. Cardenas, C. B. Poitras, M. Lipson, *Nat. Photonics* **2009**, *3*, 461.
[16] P. Alitalo, S. Tretyakov, *Mater. Today* **2009**, *12*, 22.
[17] M. Kerker, *J. Opt. Soc. Am.* **1975**, *65*, 376.
[18] A. Alu, N. Engheta, *Phys. Rev. E* **2005**, *72*, 016623.
[19] A. Alu, N. Engheta, *Opt. Express* **2007**, *15*, 3318.
[20] M. G. Silveirinha, A. Alù, N. Engheta, *Phys. Rev. B* **2008**, *78*, 075107.
[21] M. Selvanayagam, G. V. Eleftheriades, *Phys. Rev. X* **2013**, *3*, 041011.
[22] P. Alitalo, F. Bongard, J.-F. Zürcher, J. Mosig, S. Tretyakov, *Appl. Phys. Lett.* **2009**, *94*, 014103.
[23] B. Zhang, Y. Luo, X. Liu, G. Barbastathis, *Phys. Rev. Lett.* **2011**, *106*, 033901.
[24] B. Orazbayev, N. Mohammadi Estakhri, A. Alù, M. Beruete, *Adv. Opt. Mater.* **2017**, *5*, 1600606.
[25] M. Wei, Q. Yang, X. Zhang, Y. Li, J. Gu, J. Han, W. Zhang, *Opt. Express* **2017**, *25*, 15642.
[26] Nicolae-Alexandru, P. Nicorovici, G. W. Milton, R. C. McPhedran, L. C. Botten, *Opt. Express* **2007**, *15*, 6314.
[27] F. Zhou, Y. Bao, W. Cao, C. T. Stuart, J. Gu, W. Zhang, C. Sun, *Sci. Rep.* **2011**, *1*, 78.
[28] B. Orazbayev, N. M. Estakhri, M. Beruete, A. Alu, *Phys. Rev. B* **2015**, *91*, 195444.
[29] T. Kan, A. Isozaki, N. Kanda, N. Nemoto, K. Konishi, H. Takahashi, *Nat. Commun.* **2015**, *6*, 8422.
[30] W. Zhu, A. Liu, T. Bourouina, D. Tsai, J. Teng, X. Zhang, G. Lo, D. Kwong, N. Zheludev, *Nat. Commun.* **2012**, *3*, 1274.
[31] P. Pitchappa, C. P. Ho, P. Kropelnicki, N. Singh, D.-L. Kwong, C. Lee, *Appl. Phys. Lett.* **2014**, *104*, 201114.
[32] M. Manjappa, P. Pitchappa, N. Singh, N. Wang, N. I. Zheludev, C. Lee, R. Singh, **2018**, arXiv:1803.00594.
[33] L. Cong, P. Pitchappa, C. Lee, R. Singh, *Adv. Mater.* **2017**, *29*, 1700733.
[34] H. Tao, A. C. Strikwerda, K. Fan, W. J. Padilla, X. Zhang, R. Averitt, *Phys. Rev. Lett.* **2009**, *103*, 147401.
[35] P. Pitchappa, M. Manjappa, H. N. S Krishnamoorthy, Y. Chang, C. Lee, R. Singh, *Appl. Phys. Lett.* **2017**, *111*, 261101.
[36] P. Pitchappa, M. Manjappa, C. P. Ho, R. Singh, N. Singh, C. Lee, *Adv. Opt. Mater.* **2016**, *4*, 541.
[37] W. J. Padilla, A. J. Taylor, C. Highstrete, M. Lee, R. D. Averitt, *Phys. Rev. Lett.* **2006**, *96*, 107401.
[38] H-T. Chen, J. F. O'Hara, A. K. Azad, A. J. Taylor, R. D. Averitt, D. B. Shrekenhamer, W. J. Padilla, *Nat. Photonics* **2008**, *2*, 295.
[39] M. Manjappa, Y. K. Srivastava, A. Solanki, A. Kumar, T. C. Sum, R. Singh, *Adv. Mater.* **2017**, *29*, 1605881.
[40] S.-Y. Chiam, R. Singh, C. Rockstuhl, F. Lederer, W. Zhang, A. A. Bettiol, *Phys. Rev. B* **2009**, *80*, 153103.
[41] M. Manjappa, S.-Y. Chiam, L. Cong, A. A. Bettiol, W. Zhang, R. Singh, *Appl. Phys. Lett.* **2015**, *106*, 181101.
[42] M. Manjappa, S. P. Turaga, Y. K. Srivastava, A. A. Bettiol, R. Singh, *Opt. Lett.* **2017**, *42*, 2106.
[43] M. Manjappa, Y. K. Srivastava, R. Singh, *Phys. Rev. B* **2016**, *94*, 161103(R).
[44] P. Pitchappa, C. P. Ho, L. Dhakar, Y. Qian, N. Singh, C. Lee, *J. Microelectromech. Syst.* **2015**, *24*, 525.
[45] X. Chen, T. M. Grzegorczyk, B.-I. Wu, J. Pacheco Jr., J. A. Kong, *Phys. Rev. E* **2004**, *70*, 016608.

